Clays and Clay Minerals, Vol. 46, No. 3, 301–316, 1998.

ANALYTICAL ELECTRON MICROSCOPY IN CLAYS AND OTHER PHYLLOSILICATES: LOSS OF ELEMENTS FROM A 90-nm STATIONARY BEAM OF 300-keV ELECTRONS

CHI MA,[1]† JOHN D. FITZGERALD,[2] RICHARD A. EGGLETON[1] AND DAVID J. LLEWELLYN[3]

[1] Cooperative Research Center for Landscape Evolution and Mineral Exploration, Department of Geology, Australian National University, Canberra, ACT 0200, Australia

[2] Research School of Earth Sciences, Australian National University, Canberra, ACT 0200, Australia

[3] Electron Microscopy Unit, Australian National University, Canberra, ACT 0200, Australia

Abstract—Diffusion of alkali and low-atomic-number elements during the microbeam analysis of some silicates by analytical electron microscopy (AEM) has been known for some time. Our repeated analyses at 300 kV of kaolinite, halloysite, smectite, biotite, muscovite and pyrophyllite, however, showed differential loss (relative to Si) of not only alkali elements (such as K, Na, Mg) and low-atomic-number elements (such as Al) but also higher-atomic-number elements (such as Fe, Ti). For AEM of these phyllosilicates, a Philips EM430/EDAX facility with a tungsten filament was used to provide a current of 0.3 nA in a stationary beam of nominal diameter 90 nm. The loss of Al in kaolin minerals during analysis is particularly severe. Kaolin crystals can be damaged by the electron irradiation over several seconds, making it the most sensitive clay to the electron beam; in general, relative phyllosilicate stabilities are kaolin < smectite < pyrophyllite < mica. A clear dependence of element loss on crystallographic orientation has been observed for layer silicates in our study; a greater element loss occurred when the plane of the specimen foil was perpendicular to the basal planes of the phyllosilicate crystals than when the foil was parallel to the basal planes. Lower beam current, larger beam diameter and thicker specimens all reduce the loss of elements. The initial stage of irradiation produces highest rates of element loss and the rate of loss can be fitted by an exponential decay law. The analyses at low temperature of phyllosilicates showed that element loss remains serious in our analytical conditions. Since the element loss appears to be instrument- and method-dependent, one should use closely related, well-characterized phyllosilicates as compositional standards to calibrate any AEM instrument that is to be used to analyze unknown phyllosilicates, and the standards and unknowns should be analyzed under identical conditions.

Key Words—Analytical Electron Microscopy, Clay Minerals, Diffusion, Element Loss, Low Temperature, Phyllosilicates, Sputtering, Stationary Beam.

INTRODUCTION

Preferential loss of alkali elements and low-atomic-number elements, such as K, Na and Al, by AEM gives rise to anomalously low count rates for those elements and may cause significant problems in the analysis of geological specimens (Mackinnon and Kaser 1987; van der Pluijm et al. 1988; Peacor 1992). In a conventional transmission electron microscope (TEM) at accelerating voltages of 100–300 kV, electron beam damage for the common clays is very rapid (< 20 s). With a focused probe for X-ray analyses, the damage rate is exacerbated by a high current density and usually results in the loss of some elements during X-ray collection and consequent analytical errors. Losses can often be avoided by sacrificing some spatial resolution by beam scanning (scanning transmission electron microscopy [STEM], Peacor 1992) or beam defocusing.

In our study using a stationary beam of 300-keV electrons, the loss of elements in clay minerals was found to be much more serious than in other sheet silicates analyzed in the same way. The loss of Al in kaolin minerals is particularly severe, the structure of kaolin being damaged by our electron beam within 10 s. Among clays, kaolin minerals are most sensitive to the electron beam (Robertson and Eggleton 1991; Ma and Eggleton 1994; Ma 1996).

In this paper, the problems associated with AEM analysis in TEM mode for Al, K, Mg, Ca and Fe in kaolin and other phyllosilicates are presented and compared. In particular, the variation of results as a function of the electron beam diameter, the specimen thickness and the crystallographic orientation of the sample plane are discussed. A preferred procedure for obtaining reliable analyses is also presented.

EXPERIMENTAL

Analyses were obtained in a Philips EM430 TEM at an accelerating voltage of 300 kV with an attached solid-state, low-takeoff-angle (15°) energy-dispersive X-ray (EDS) detector.

For analysis, the sample was tilted 30° toward the X-ray detector. A tungsten filament was used for all spectra collection and provided 1.95×10^9 electrons

† Plesent adress: Division of Geological and Planetary Sciences, California Institute of Technology, Pasadena, California 91125.

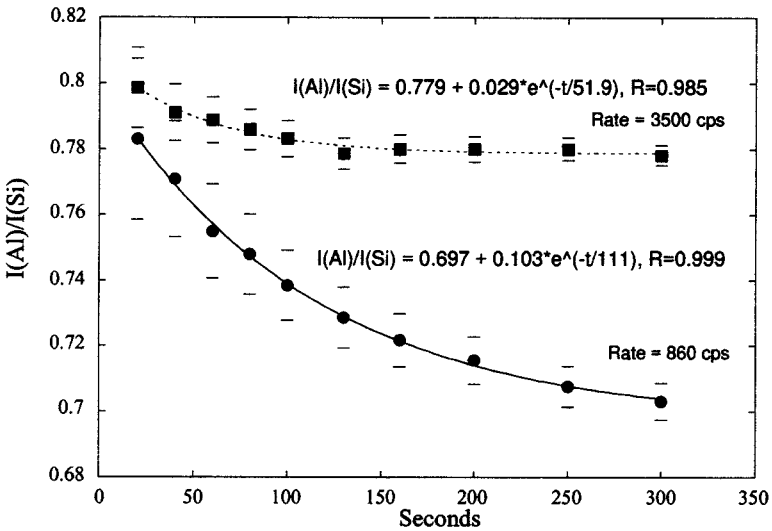

Figure 1. An example (kaolinite) showing the decreasing ratio of Al versus Si X-rays detected for increasing live time of analysis for constant probe current and sample position. The error bar for each analysis point has been calculated using simple square-root counting statistics for total integrated counts of both peak and background in the energy region of interest. The exponential correlation lines (fitted parameters and correlation coefficient shown) are well within the uncertainty range.

per second (a beam current of 0.3 nA) at the sample for a nominal beam diameter of 90 nm. In addition, some data at a defocused beam diameter of 350 nm were obtained for comparison.

The clay minerals kaolinite, halloysite and smectite, and other phyllosilicates pyrophyllite, muscovite and biotite were studied. Their chemical compositions and sample locations are given in Table 1. Samples were prepared in 1 of 3 ways: 1) particles dispersed on a carbon film supported by a copper grid so most (001) planes of platy phyllosilicates lay parallel to the film, 2) sectioning with a diamond microtome to produce slices normal to the (001) plane or 3) ion milling, which allows the study of any specimen thickness effect on the analysis of clay minerals by AEM. The role of the crystallographic orientation in the analytical procedure was examined using platy kaolinite and biotite.

Cliff and Lorimer (1975) established the following equation for "thin-film" AEM in which atomic number and X-ray absorption and fluorescence effects are insignificant:

$$C_a/C_b = k_{ab}(I_a/I_b) \quad [1]$$

where C_a and C_b are the weight concentrations of elements a and b, I_a and I_b are the intensities of emission lines of those elements, and k_{ab} is a proportionality factor that is a function of parameters concerned with beam/specimen interaction and detector efficiency.

In an alternative formulation:

$$C'_a/C'_b = k'_{ab}(I_a/I_b) \quad [2]$$

where C'_a and C'_b are the atomic concentrations of elements a and b. Ideally, k'_{ab} is a constant independent of measuring time and can be routinely calibrated using standards of known composition for the accelerating voltage of interest.

Because silicates are the most abundant group of minerals, intensity for X-ray emissions of a given element is ratioed to that of Si (Lorimer and Cliff 1976; Peacor 1992). Thus for Al:

$$k'_{Al,Si} = (C'_{Al}/C'_{Si})(I_{Si}/I_{Al}) \quad [3]$$

Ratios of intensity of Al, K, Fe, Mg, Ti relative to that of Si were measured in this study and plotted against the live time (that is, counting time corrected for detector dead time). In a similar study on clay minerals, Mackinnon and Kaser (1987) minimized uncertainty by averaging data from about 15 separate analyses. In our study, we were unable to average due to slight chemical and structural heterogeneity. Figure 1 shows the uncertainty ($\sqrt{n}$ counting statistics for total integrated peak count and for background) associated with our single analyses, and demonstrates that the curve fitted to the decay over time (described in the Discussion section) locates well within the error bounds. Since this was true for all our trends, error bars are not drawn on Figures 2 to 11.

RESULTS

Kaolinite and Halloysite

Changes in Al/Si intensity ratios were measured as a function of counting time (Figure 2) at 3 locations on an ion-milled kaolinite specimen. Different specimen thicknesses produced different count rates (that is, 860, 1600, 3500 counts per second [cps]) from a

https://doi.org/10.1346/CCMN.1998.0460309 Published online by Cambridge University Press

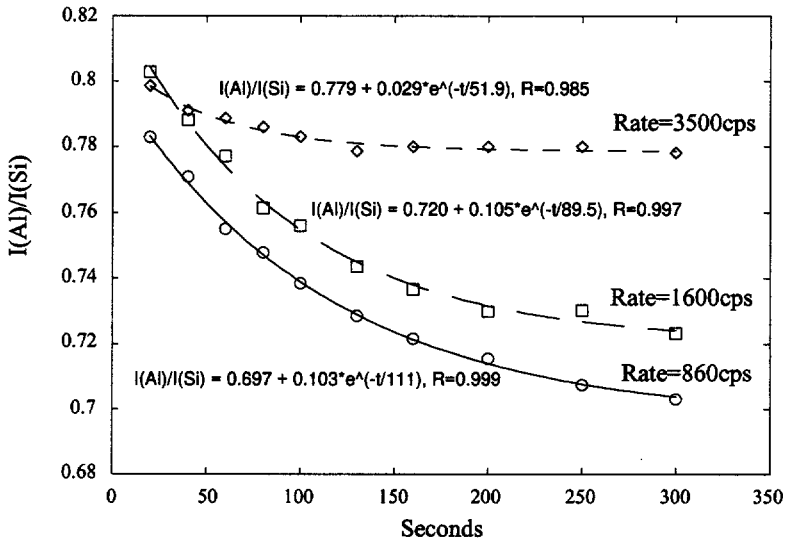

Figure 2. Al/Si intensity ratio for increasing live time of analysis for constant probe current and stationary beam at 3 different points of an ion-milled kaolinite specimen. The count rate is related to the thickness. The sample is highly ordered kaolinite (Kao I), specimen plane perpendicular to (001).

constant incident beam current. The highest rate corresponds to the thickest area (but with some spurious counts arising from the copper support grid). Figure 2 demonstrates that the relative loss of Al is greater for thinner areas.

Figure 3 shows the change in Al/Si, K/Si and Fe/Si intensity ratios with increasing counting time in a microtomed kaolinite specimen. It is evident that intensities for K and Fe decrease much more than Al (67% for K, 14% for Fe and 7% for Al). The presence of K implies that the kaolinite contains interstratified mica layers (Ma 1996).

Figure 4 shows the differential trend of Al/Si intensity ratio with changing irradiation area for a constant beam current of 0.3 nA focused to 90-nm diameter (full width, one-tenth maximum) or spread to 350-nm diameter. The loss of Al decreases when analyzing the larger area. As clearly shown in Figure 5, the crystallographic orientation of the specimen plane does affect the loss of elements in kaolinite. Aluminium loss is higher for the specimen cut perpendicular to (001).

Tubular halloysite also undergoes differential Al loss during analysis (Figure 6).

Smectite

Two types of smectite were studied. For saponite when the specimen plane was parallel to (001), the Mg/Si, Ca/Si and Fe/Si intensity ratios decreased with the counting time whereas the Al/Si ratio changed little. However, when the specimen plane was perpendicular to (001), the Al/Si ratio decreased also (Figure 7a), although direct comparison is complicated by the analyzed domains having slightly different compositions (which are Sm I and Sm II as listed in Table 1). The lower plot of Figure 7a shows the effect of thickness: the loss of Mg is greater in the thinner area. Wyoming montmorillonite (Sm III) shows only a slight differential element loss (Figure 7b).

Muscovite

Figure 8 shows that the K loss in muscovite is larger than those for Al and Fe when the (001) planes are placed perpendicular to the beam. The beam damage rate monitored from SAED patterns is much lower than that for kaolin.

Biotite

The loss of elements in biotite is orientation-dependent. Figure 9 shows that the K loss is significant in both orientations, whereas the loss of Fe, Al, (Ti and Mg) is only apparent when the specimen plane is perpendicular to (001).

Pyrophyllite

The loss of Al is evident in pyrophyllite (Figure 10), although its structure is not damaged as rapidly as that of kaolinite.

Analysis with a Cold Stage

A Gatan 636N liquid-N_2 double-tilting holder was used for low-temperature analysis. Before analyses, the holder was cooled by liquid nitrogen to a steady temperature of −170 °C, measured by a thermocouple in the solid tip of the side-entry holder. From other studies (such as Mackinnon and Kaser 1987), much lower element loss was expected during these X-ray analyses of kaolinite, smectite, muscovite and biotite. The representative results are shown in Figure 11. The

https://doi.org/10.1346/CCMN.1998.0460309 Published online by Cambridge University Press

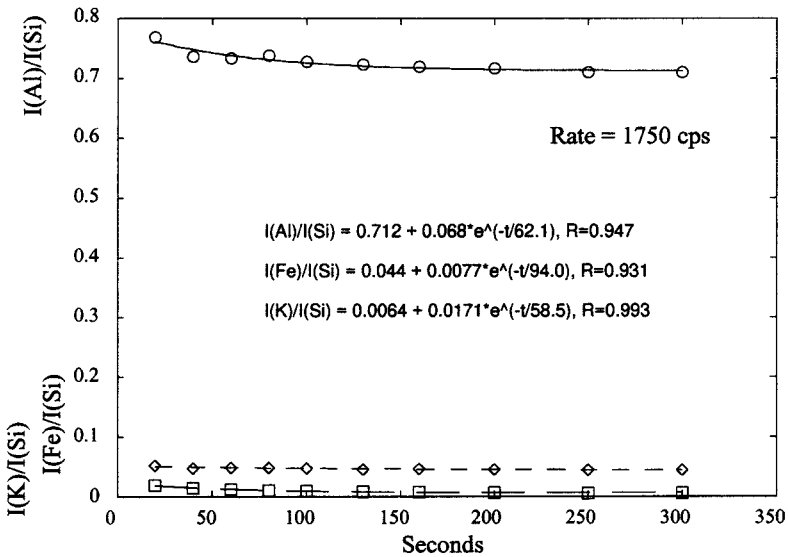

Figure 3. Al/Si, K/Si and Fe/Si intensity ratios for increasing live time of analysis for constant probe current and sample position in a microtomed specimen of medium-ordered kaolinite (Kao III), specimen plane perpendicular to (001).

loss rates of K, Al, Mg, Fe and Ca in these minerals remain similar to those measured at room temperature. For Pittong kaolinite (Kao I) (Figure 11a), the loss of Al may even have been higher at low temperature, though the lower count rate indicates that a thinner region was being analyzed.

The temperature of the analyzed region can obviously never be measured, but an attempt was made to get a better indication than provided by the thermocouple in the tip of the 636N specimen holder. A Type K thermocouple (nickel-chromium/nickel-aluminium) with small thermal mass was made from 0.2-mm diameter wires and the junction soldered to a 3-mm Cu disc of thickness 0.15 mm. This disc could be screwed into the 636N holder just like the standard holey-C or ion-milled specimens. The thermocouple/disc was calibrated crudely by measuring the electromagnetic field (emf) generated during immersion in 1) liquid N_2, 2) a bath of ethanol + solid CO_2 and 3) a bath of water + ice. The calibrated thermocouple was screwed into the 636N holder, the holder inserted into a high vacuum chamber (10^{-5} torr) and the thermocouple emf

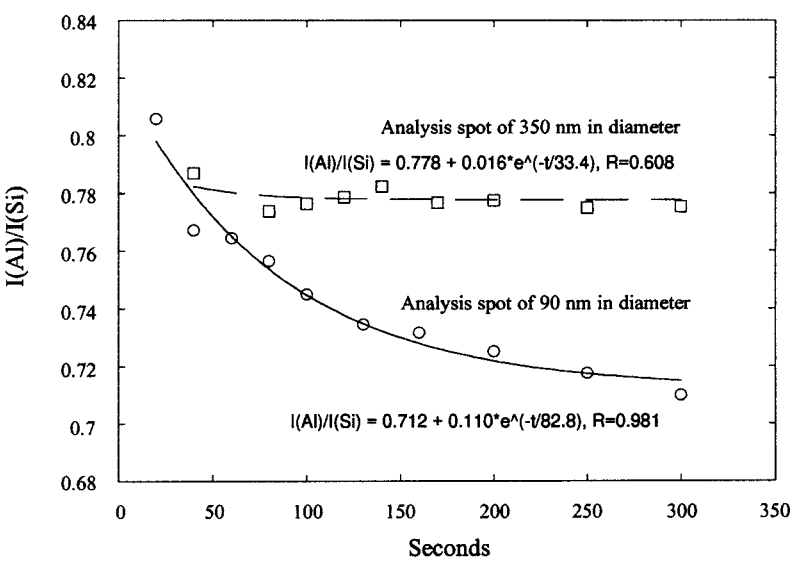

Figure 4. Al/Si intensity ratio for increasing live time of analysis for constant probe current and sample but for 2 different beam diameters in a microtomed specimen of highly ordered kaolinite (Kao II), specimen plane perpendicular to (001).

https://doi.org/10.1346/CCMN.1998.0460309 Published online by Cambridge University Press

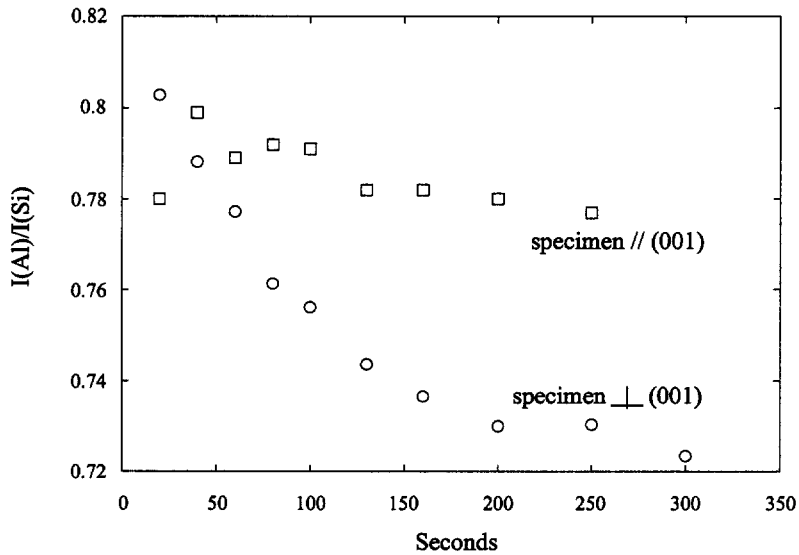

Figure 5. Al/Si intensity ratio for increasing live time of analysis for constant probe current and sample position but with 2 different orientations of specimen plane in highly ordered kaolinite (Kao I).

measured at room temperature to confirm that extra feedthrough connections did not affect voltages. Finally, with the 636N dewar filled with liquid nitrogen, the temperature of the specimen cup was measured to be −130 ± 5 °C even though the 636N controller indicated −170 °C. Clearly, samples consisting of isolated phyllosilicate crystals supported on thin C films and Cu grids are unlikely to be cooled even to −130 °C, though the thicker and continuous ion-milled specimens could be. Nevertheless, all samples must be significantly cooled in the 636N holder. For simplicity in the following, we refer to cooled temperatures of −170 °C, even though we know that the specimen temperature is at least 40 °C above this indication.

DISCUSSION

Loss of All Elements

Electron irradiation, which turns clay minerals amorphous by damaging their crystal structures, is also responsible for loss of elements during AEM analysis. Figure 12 is a typical bright field image

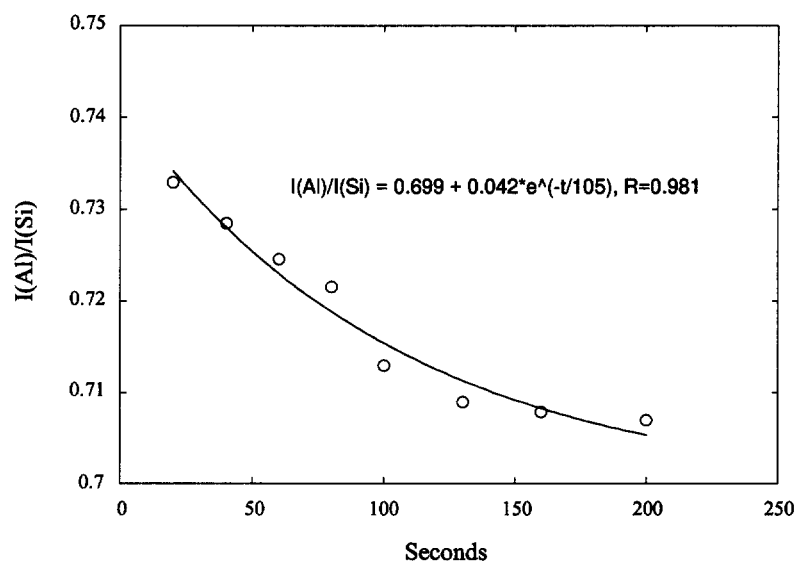

Figure 6. Al/Si intensity ratio for increasing time of analysis for constant probe current and sample position in a dispersed halloysite specimen. The sample is tubular halloysite with tubes parallel to the plane of the Cu grid.

https://doi.org/10.1346/CCMN.1998.0460309 Published online by Cambridge University Press

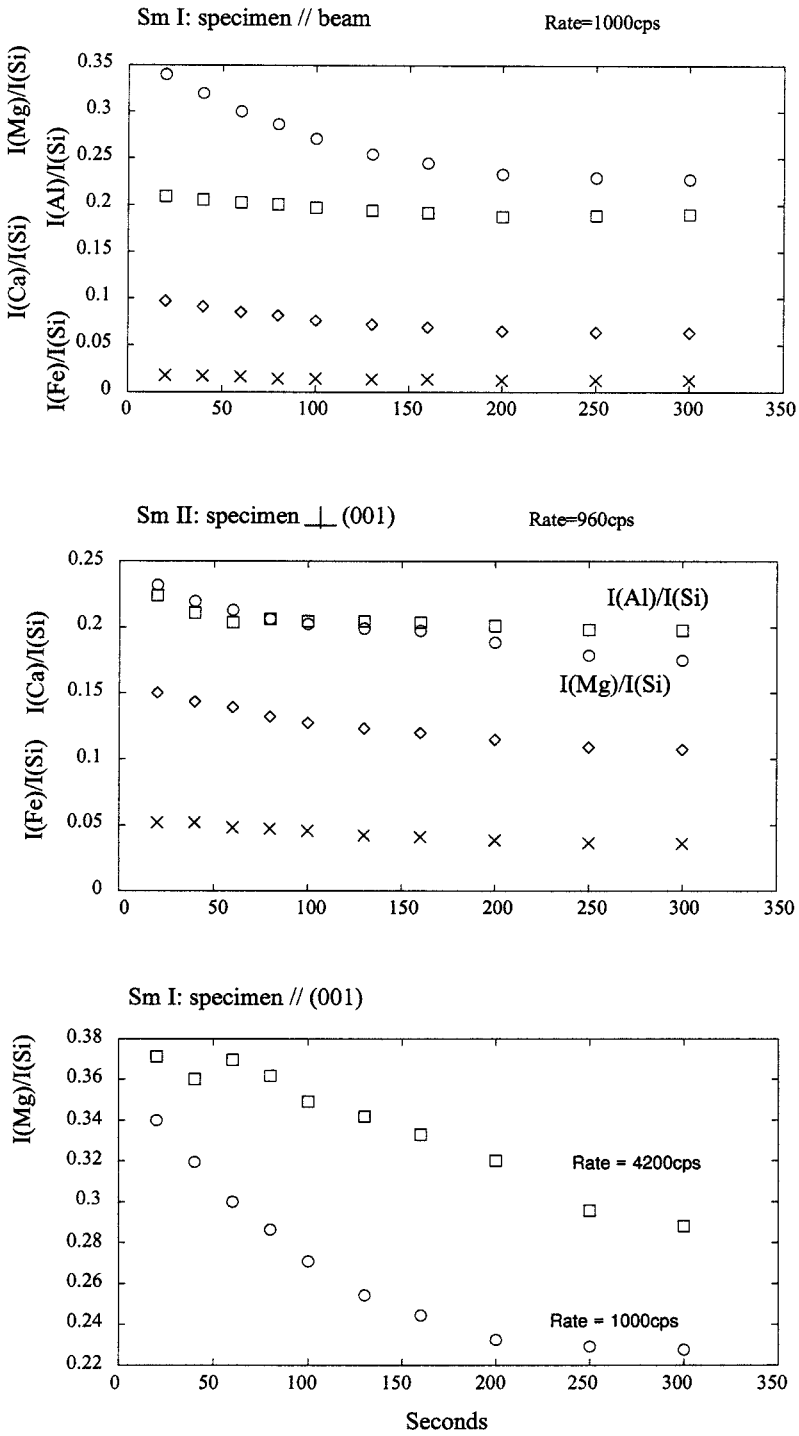

Figure 7. Mg/Si, Al/Si, Ca/Si and Fe/Si intensity ratios for increasing time of analysis for constant probe current and sample position in dispersed smectite specimens. a) Saponite (Sm I & Sm II).

https://doi.org/10.1346/CCMN.1998.0460309 Published online by Cambridge University Press

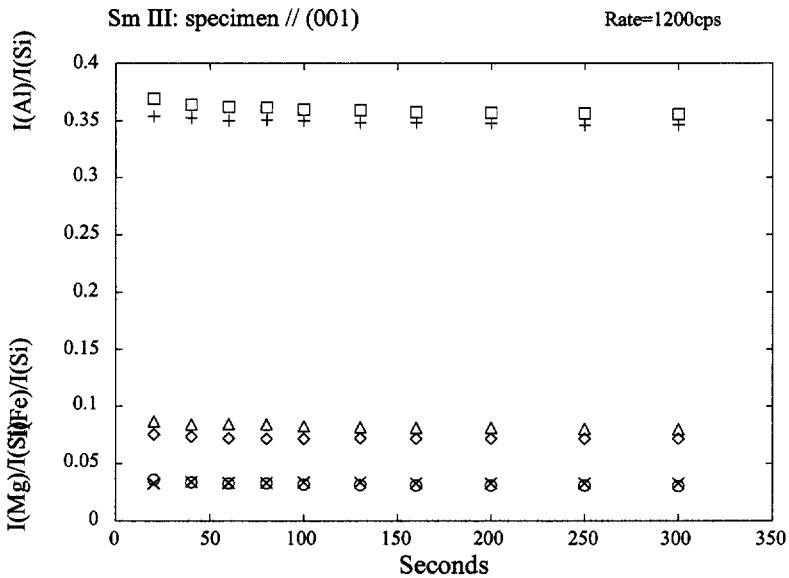

Figure 7. Continued. b) Montmorillonite.

showing a hole "drilled" in 250 s by an electron beam within a kaolinite particle. Most original components within the hole (Si, Al, O) are presumed to have been sputtered away in the form of ions, atoms and complexes though some atoms/ions could diffuse into the surrounding region. For the mechanism of element loss, the "diffusion" accompanying irradiation by 100-keV electrons described by van der Pluijm et al. (1988) may not be an adequate description under our stationary 300-kV beam, since the loss of elements involves sputtering and perhaps other phenomena.

One should be aware that during analysis all elements are differentially lost to some degree, especially when the sample is sputtered away (Figure 12). In silicates, the loss of Si seems to be lowest compared with the loss of other elements; therefore, the change of i/Si intensity ratios (i: elements other than Si) will be reflected in chemical composition calculated via the Cliff–Lorimer approach.

In the AEM analyses of Ahn et al. (1986) at 100 kV, only the alkali element concentrations of micas changed significantly during exposure to the electron beam at room temperature. The effect was particularly marked in Na- and K-muscovites and gave rise to characteristic mottled or fissured textures. Similar microstructures were shown by Knipe (1979) and Peacor (1992). Loss of low-atomic-number (low-Z) elements by AEM at 200 kV for some clays (kaolinite and smectite) was reported by Mackinnon and Kaser (1987). In our study, we found that even Fe (and possibly Ti) concentrations also change significantly in some phyllosilicates under certain conditions at 300 kV (see Figure 9). It seems that element loss increases with accelerating voltage, though it is impossible to make a quantitative comparison since the other experimental conditions used in this study and those previously are different. However, it is evident that sputtering damage is significant using a stationary beam at 300 kV, as well as diffusion. This is of importance in our understanding of "element loss".

Selection of larger analysis areas also reduces the loss of elements for stationary probes. For example, in kaolinite (see Figure 4), the Al/Si ratio changes only slightly throughout the analysis using the defocused beam of 350-nm diameter, but clearly decreases for the focused beam 90 nm in diameter. Therefore, to use analysis areas as large as possible is particularly significant and important for clay minerals. When the beam area is set to totally enclose the individual analyzed grain, the element loss still exists in some of our AEM analyses on isolated kaolin particles. This might imply that diffusion is not the only primary loss mechanism under our experimental conditions.

Crystallographic Orientation Effect

The element loss from kaolinite studied by Mackinnon and Kaser (1987) was based on samples dispersed over holey carbon film on Be grids. In our study, both microtomed sections and ion-milled specimens were used in addition to dispersed samples for studying any crystallographic orientation effect. Figure 5 shows that, in kaolinite, loss of Al is dependent on crystal orientation; greater Al loss occurs when the specimen plane is perpendicular to (001) compared to when the specimen is parallel to (001).

K is lost similarly during analysis of mica specimens, for specimen planes both parallel and perpendicular to (001). In biotite, significant losses of Fe and

https://doi.org/10.1346/CCMN.1998.0460309 Published online by Cambridge University Press

Table 1. Chemical composition of kaolinite, halloysite, smectite, biotite, muscovite and pyrophyllite.

†,‡	Kao I	Kao II	Kao III	Hall	Sm I	Sm II	Sm III	Mus	Bio	Pyr
SiO_2	47.49	48.94	45.70	48.31	50.92	52.39	63.24	45.85	37.13	66.60
Al_2O_3	38.34	36.73	38.37	36.92	13.62	20.85	23.44	32.35	17.93	28.84
TiO_2	0.00	0.00	—	—	0.03	—	—	—	1.62	—
FeO	0.21	0.34	2.54	0.78	0.50	2.10	3.98	3.40	20.74	—
MgO	—	—	—	—	25.85	11.64	2.30	—	7.19	—
MnO	—	—	—	—	—	—	—	—	0.37	—
CaO	—	—	—	—	2.76	2.08	—	—	—	—
Na_2O	—	—	—	—	—	—	2.30	0.76	—	—
K_2O	—	—	—	—	—	—	—	10.83	10.33	—
Total	86.03	86.00	86.60	86.00	93.67	89.05	95.75	93.19	95.31	95.44
O,OH§	7	7	7	7	11	11	11	11	11	11
Si	1.97	2.10	1.98	2.08	3.34	3.54	3.91	3.16	2.86	3.98
Al(IV)	0.03	—	0.02	—	0.66	0.46	0.09	0.84	1.14	0.02
Al(VI)	1.99	1.86	1.94	1.87	0.39	1.20	1.62	1.80	0.48	2.01
Ti	—	—	—	—	—	—	—	0.00	0.08	—
Fe	0.01	0.02	0.09	0.04	0.03	0.12	0.21	0.19	1.35	—
Mg	—	—	—	—	2.52	1.17	0.24	—	0.83	—
Mn	—	—	—	—	—	—	—	—	—	—
Ca	—	—	—	—	0.19	0.15	—	—	—	—
Na	—	—	—	—	—	—	0.28	0.11	—	—
K	—	—	—	—	—	—	—	0.96	0.83	—

These EDS measurements were made using a JEOL 6400 SEM with a defocused beam of 15-kV electrons.

† Kao = kaolinite; Hall = halloysite; Sm = smectite; Mus = muscovite; Bio = biotite; Pyr = pyrophyllite.

‡ Kao I: PONG4, Pittong, Vic.; Kao II: E2, CMS; Kao III: G1500, Weipa, Qld.; Hall: Mt. Morgan, Qld.; Sm I & Sm II: saponite, Cooma, NSW; Sm III: montmorillonite, Wyoming, USA; Mus: Philadelphia, USA; Bio: Harts Range, NT; Pyr: from ANU Geology Department Museum.

§ Numbers of equivalent 2+ anions [based on $O_5(OH)_4$ for Kao and Hall, and $O_{10}(OH)_2$ for Sm, Mus, Bio and Pyr] used as the basis for calculating the mineral formulae expressed as cation numbers below.

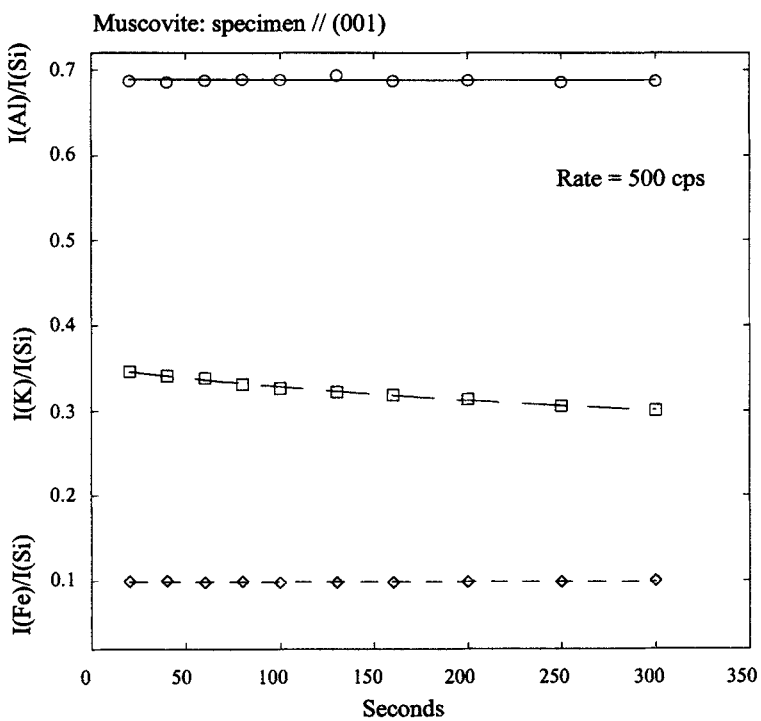

Figure 8. K/Si, Al/Si and Fe/Si intensity ratios for increasing time of analysis for constant probe current and sample position in a dispersed muscovite specimen, specimen plane parallel to (001).

https://doi.org/10.1346/CCMN.1998.0460309 Published online by Cambridge University Press

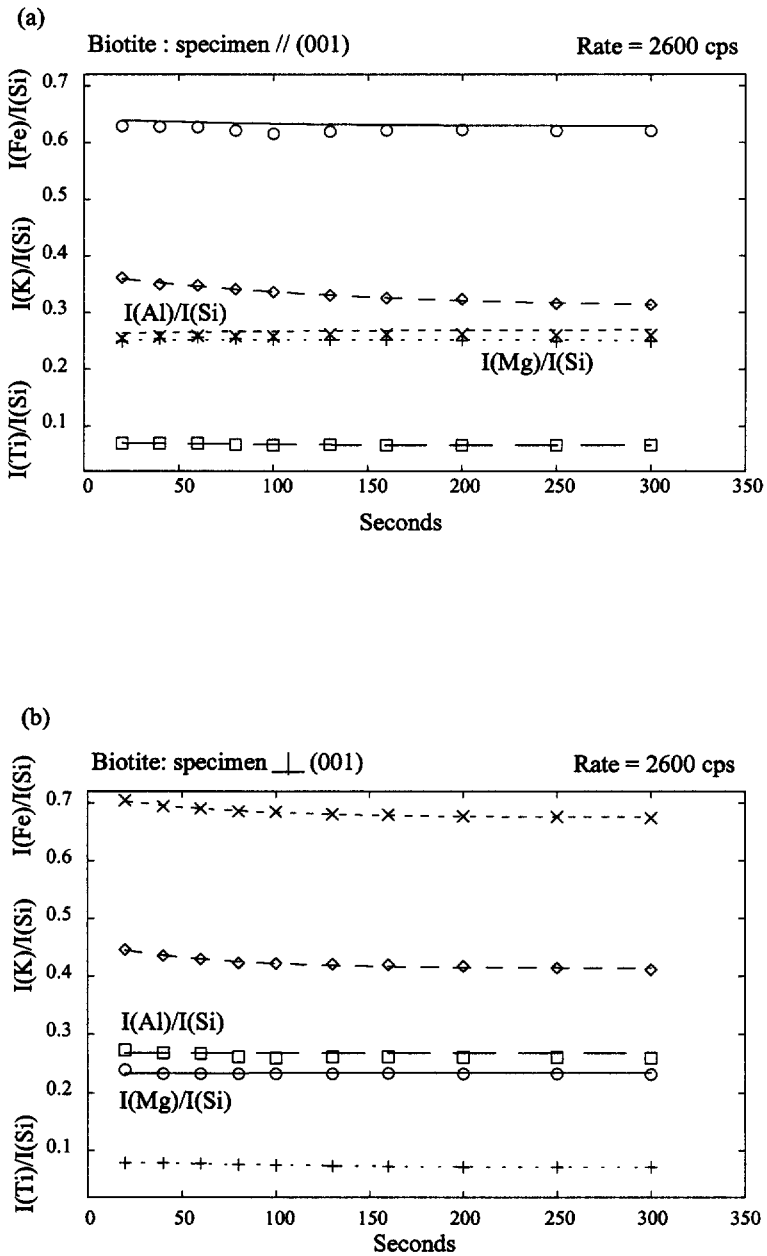

Figure 9. K/Si, Al/Si and Fe/Si intensity ratios for increasing time of analysis for constant probe current and sample position in a dispersed biotite specimen, a) specimen plane parallel to (001), b) specimen plane perpendicular to (001). Rate = 2600 cps.

Al occur only in specimens cut perpendicular to (001) (see Figure 9). This indicates some dependence upon the crystal structure.

We must highlight that the orientation effect cannot have its origins in channelling-enhanced X-ray emission. While this effect has been well known (Williams and Carter 1996), it can be discounted as a major phenomenon affecting our measurements. This is because for analysis all samples were tilted 30° about the sample rod, an axis with a random orientation relative to the individual crystal's axes. Thus, for samples cut parallel to (001), the beam direction during analysis is 30° removed from [001], but in an unspecified direction. Likewise, for samples cut perpendicular to (001), after tilting randomly by 30°, only very few would show strong *(00l)* diffraction. Therefore, in no crystal would the electron beam have been parallel to a major zone axis during anal-

https://doi.org/10.1346/CCMN.1998.0460309 Published online by Cambridge University Press

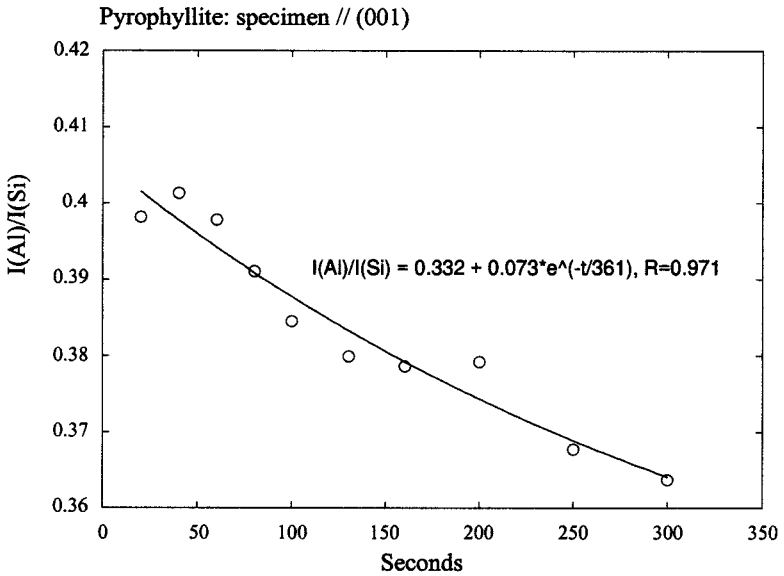

Figure 10. Al/Si intensity ratio for increasing time of analysis for constant probe current and sample position in a dispersed pyrophyllite specimen, specimen plane parallel to (001).

ysis, and only a few would have been oriented for strong Bragg diffraction.

Under reproduced TEM conditions including similar specimen thickness, a crystal with its specimen plane parallel to (001) is less beam sensitive (more resistant) than one that is perpendicular to (001). We also observed generally that *hk0* diffractions disappeared more slowly than did *hkl* diffractions. This broadly agrees with the specimen orientation effect on the measured loss of elements. A reason for this could be that less energy is needed to disrupt truncated, weakly bonded layers whereas more energy is needed to remove part of the crystal in which extensive sheets are strongly bonded, as illustrated in Figure 13. In addition, possibly the beam energy disrupts the interlayer, allowing K loss, destroying the periodicity parallel to [001], but leaving the *hk0* plane less disordered. Our measurements on the orientation effect are opposite to the observations of van der Pluijm et al. (1988).

Element loss from kaolinite shows an equivalent dependence on orientation with higher Al loss when the specimen plane is perpendicular to (001). Kaolinite in either orientation is damaged much faster (in less than 10 s in general) than all other layer silicates.

Finally, the effect of crystallographic orientation in the analysis of clay minerals cannot be evaluated when the analysis area is very thin because rapid damage masks the effect.

Effect of Crystal Ordering and Defects

Most common clay minerals, such as kaolinite, smectite and illite, occur as submicrometer crystallites with varying degrees of structural order and may be as thin as 1 or 2 unit cell dimensions along [001]. The present study considered the effect of overall crystal defect state that may also be significant in controlling the loss of elements at the early stage of an analysis in clay. It is known that clay minerals are the most electron-beam-sensitive phyllosilicate, and kaolin is the most sensitive clay mineral (Mackinnon and Kaser 1987; Robertson and Eggleton 1991; Ma and Eggleton 1994; Ma 1996). Kaolinite and halloysite can only "survive" for less than 10 s in normal image mode under TEM before their electron diffraction patterns disappear. Highly ordered kaolinite can survive for a little longer than poorly ordered kaolinite (Ma 1996). For an analysis by AEM, a counting time of 50 s or greater (to achieve acceptable counting statistics) is required. Therefore, the majority of X-ray emissions collected for analysis using a stationary electron probe probably arise from a phase that has been highly disordered *in situ* relative to the original clay crystal. It is apparent that the Al/Si intensity ratios of the highly ordered kaolinite from Pittong are higher than those of the less-ordered kaolinite from Weipa (see Figures 2 and 3, Al/Si data for count rate ~1600 cps) even though their compositions are very similar (Kao I and Kao III, Table 1). This implies that differential element loss is more serious in less-ordered crystals. Therefore, crystal ordering and defects do play a significant role in element loss, particularly at the earlier stage of an analysis. However, the effects of disorder in AEM analyses of clay may be masked to some degree by rapid damage rates.

Peacor (1992; personal communications) showed that the grade of diagenesis is reflected by the rate of

https://doi.org/10.1346/CCMN.1998.0460309 Published online by Cambridge University Press

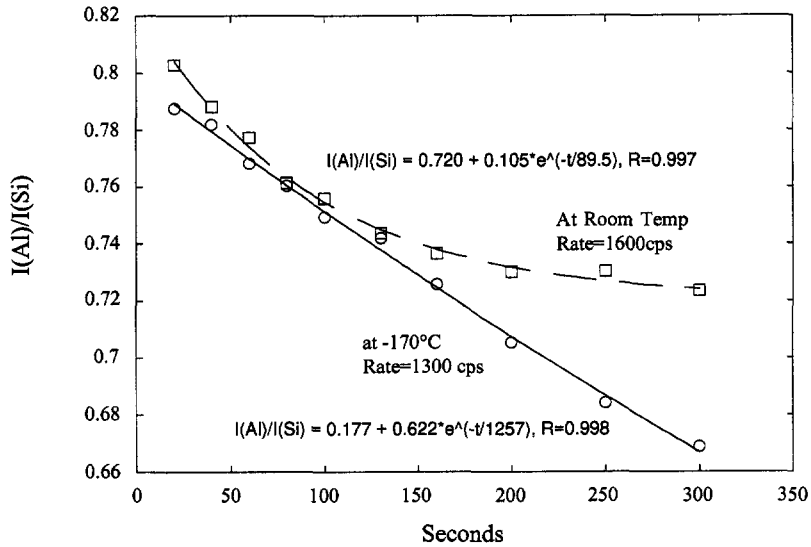

Figure 11. Loss of elements when using a cold stage. a) Kaolinite (Kao I).

element loss: K loss is negligible in 2M muscovite but becomes increasingly greater as one goes to illite and ultimately to smectite with decreasing grade. Selected area electron diffraction (SAED) patterns were not reported to change for those minerals under AEM conditions of 100 (or 120) kV accelerating voltage and scanning probe mode. Peacor attributed the change in K-loss to be due to change in degree of disorder as evidenced in part by variations in lattice fringes and in dislocation densities. We have observed the same in kaolin group minerals analyzed at 300 kV with stationary probe, although the damage rates for highly ordered crystal may be so rapid that the initial state of disorder is rapidly overprinted.

Morphology Effect

It is possible that morphology affects the degree of element loss at the very beginning of an analysis on a kaolin particle (within 10 s), although the rapid damage by a focused beam may mask any such morphological effect. An analysis spot of 90 nm in diameter damaged both the platy and tubular kaolins' structure in about 3–5 s, similar to the loss of Al in kaolin with a different morphology (Figures 2 and 6).

Effects of Different Analytical Conditions and Techniques

LOW TEMPERATURE. Mackinnon and Kaser (1987) and Mackinnon (1990) demonstrated that low temperature reduces the rate of element loss on AEM of clay minerals when a 200-kV stationary beam was used. Although we used a cold stage similar to that used by Mackinnon and Kaser (1987), we could not reproduce any strong effect (Figure 11). We took care to verify that our Gatan 636N stage was indeed cooling the sample region by directly measuring a specimen cup temperature around −130 °C. We suppose that the higher accelerating voltage (300 kV) we used could be responsible for overwhelming the effect of low temperature.

OTHER CONDITIONS. Comparison of the analytical results on phyllosilicates by Peacor (1992, scanning beam analyses at 100 or 120 kV), Mackinnon and Kaser (1987, stationary beam, 200 kV) and our own (stationary beam, 300 kV) illustrate the complexity of AEM analyses of these sensitive minerals. Results range from minimal or zero loss of elements by Peacor to serious loss of elements in our measurements. Part of the explanation will lie in the use of a scanning beam by Peacor, although we must point out that the beam selected for analyses in our EM430 (LaB_6 filament, low beam current 0.3 nA and microprobe-mode beam diameter 90 nm) is not particularly severe relative to microbeams used in most modern AEM studies. However, the fact that the 350-nm beam diameter reduced our element loss shows that current densities were still excessive. However, X-ray counting rates on the order of 1000 cps are the minimum required to give acceptable analytical precision over 100-s counting times, so we could not sensitively analyze with any lower beam current using our detector with a solid angle of collection of 0.13 steradians. The alternative, to defocus the 300 kV beam to several hundred nanometers in diameter, is also undesirable since it defeats the purpose of turning from the electron microprobe (thick specimen) to the AEM (thin film) for improved spatial resolution. We submit that our results, put in

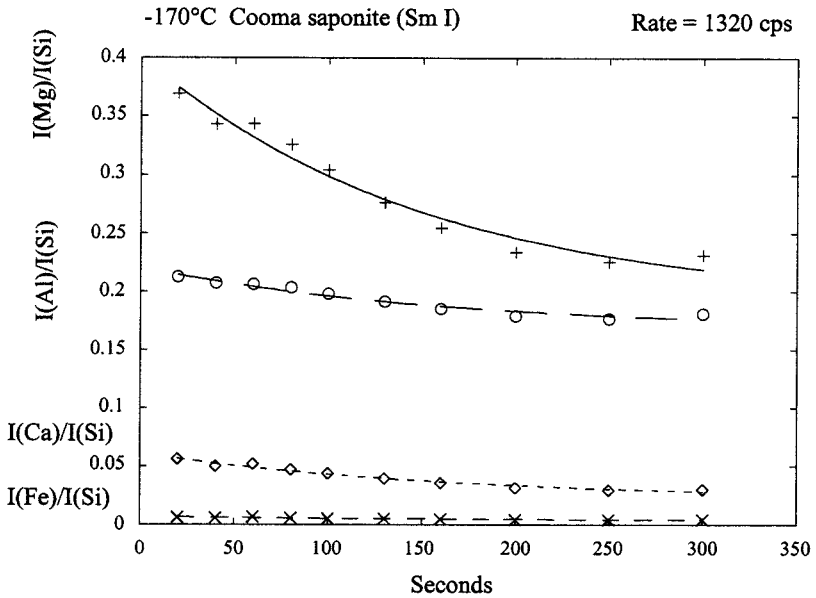

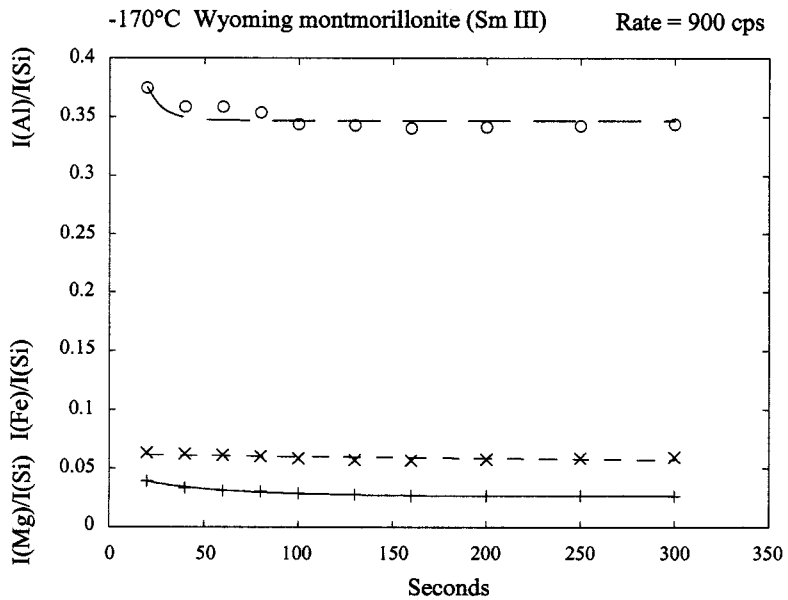

Figure 11. Continued. b) Smectite (Sm I and Sm III).

the context of other studies, emphasize the need for phyllosilicate mineralogists to carefully select their analytical conditions when embarking on AEM studies.

Correlation between $I_{(i)}/I_{(Si)}$ and Measuring Time

All our element-loss data could be fitted by an exponential correlation between the ratio $I_{(i)}/I_{(Si)}$ and measuring time during an analysis on a constant spot (as illustrated in Figures 1 to 4, 6, 9, 10 and 11). The correlation line locates within the error range as demonstrated in Figure 1. The general expression of the ratio $I_{(i)}/I_{(Si)}$ with time is:

$$I_{(i)}/I_{(Si)} = K_3 + K_1 e^{K_2 t} \quad [4]$$

where K_1, K_2 and K_3 are constants and t is counting time. This equation may suggest that there are 2 parts

https://doi.org/10.1346/CCMN.1998.0460309 Published online by Cambridge University Press

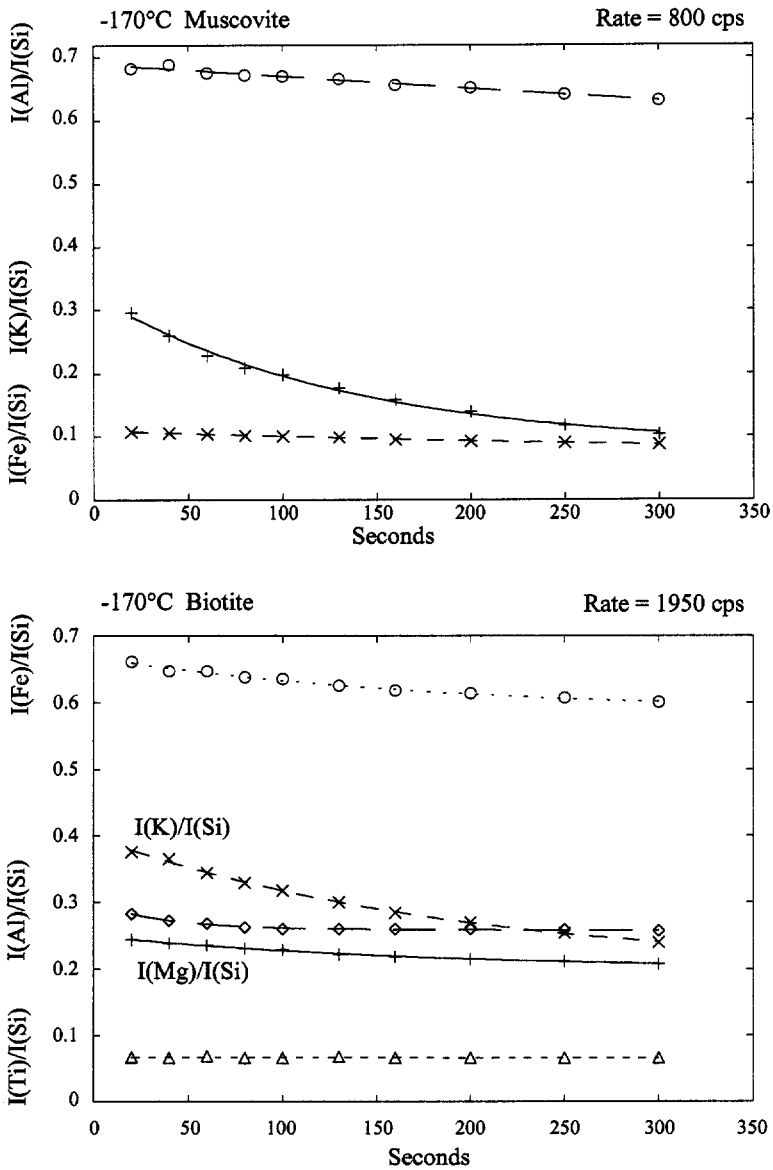

Figure 11. Continued. c) Muscovite. d) Biotite.

which can be attributed to the intensity ratios; that is, one ($K_1e^{K_2t}$) that decays and another (K_3) that does not.

Loss of material by electron beam damage gives rise to a reduction in X-ray ratio following an exponential decay curve. The effect of electron distribution on the analysis area is likely to contribute to such a relation (Figure 14). Figure 14 shows that the main mechanisms expected for the loss of elements are likely sputtering and "diffusion". The atom displacement within the analysis area is unlikely to affect element losses very much. However, how or why the exponential relation occurs is not clear, although the ($K_1e^{K_2t}$) part is suspected to relate to diffusion whereas the (K_3) part is probably caused by sputtering. Perhaps the exponential relation could be used in future as an index of structural stability in phyllosilicate minerals.

Determination of Clay Composition

Because of the differential loss of elements during AEM analysis as mentioned above, clay compositions calculated using fixed *k*-factors (calibrated from beam-stable minerals other than clay, such as feldspars) generally show a small excess of Si compared to its ideal composition and a corresponding deficiency in Al and other elements such as Fe. Two methods were proposed and developed in this study to overcome this

https://doi.org/10.1346/CCMN.1998.0460309 Published online by Cambridge University Press

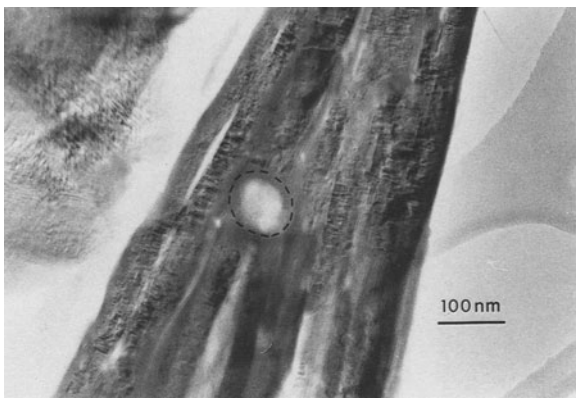

Figure 12. TEM image showing a hole within a kaolinite particle, which was drilled by an electron beam during 1 analysis (250 s). The hole is 70 nm in diameter and the analysis spot marked by a dashed circle is 90 nm in diameter.

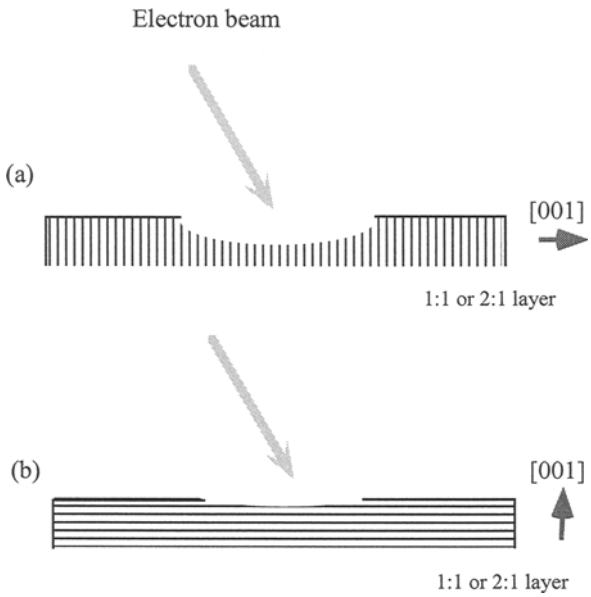

Figure 13. Sketch showing the possible electron disruption on sheet silicates. a) When the specimen plane is perpendicular to (001), less energy is needed to disrupt the truncated basal-plane layers, which leads to rapid sputtering. b) When the specimen plane is parallel to (001), more energy is needed to disrupt and remove extensive, strongly bonded sheets.

problem and increase the reliability of results. The methods are described as follows using kaolinite as an example.

METHOD 1. "Effective" *k*-factors of Al/Si and Fe/Si are obtained using well-known kaolinites; these values will be analysis-time dependent. Then the "effective" *k*-factors are used accordingly to calculate compositions of unknown kaolinites where these analyses are obtained under exactly the same conditions (including beam current, diameter, sample thickness and crystal orientation) as were used for the standards. Figure 15, as an example, illustrates the "effective" *k*-factors of Al/Si as a function of analysis time and at 3 different thicknesses for well-ordered kaolinite with its specimen plane perpendicular to (001).

METHOD 2. First, a series of measurements should be made of the X-ray intensities as a function of time of an unknown kaolinite, just like the analyses in the Results section. Then the intensity ratios (such as Al/Si and Fe/Si) of this unknown phase at time zero are estimated using their exponential correlation lines. The composition of the unknown kaolinite is finally calculated by using conventional *k*-factors which can have been determined from any compositionally characterized solid. However, uncertainty does arise as shown for example in Figure 2 where it is clear that the time-zero intensity ratios of Al/Si (that is, $K_1 + K_3$) vary from 0.80 to 0.83, although this may be caused by original chemical heterogeneity between kaolinite crystals. Atomic Al/Si ratios convert to 0.936, 0.945 and 0.936 for the 3 analyses when using the conventional *k*-factor ($k = 1.17$).

Both methods are very time-consuming. Table 2 shows the actual analysis of the Pittong kaolinite (Kao I) and the AEM analysis using methods 1 and 2. Method 1 clearly produces better results.

CONCLUSIONS

The effects of direct atom displacement, ionization and heating during electron bombardment of layer silicates give rise to specimen damage that can cause serious AEM analysis errors resulting from the differential loss of elements.

1) In our analysis of phyllosilicates, not only alkali elements and low-Z elements but also Fe are significantly lost over time. The degree of loss of Al in kaolinite is greater than in other sheet silicates, much higher even than the K loss in muscovite, for example.

2) The rate of element loss is in part a function of structure and composition. The element loss in clay minerals is suggested (mainly) to be due to diffusion and sputtering. Early in the structural damage period, diffusion could be the main cause for the element loss together with sputtering, whereas during the later stages (after the structure has been lost) sputtering could dominate. However, this might be different for other phyllosilicates (such as muscovite and biotite) where diffusion could be the major factor for much longer because these minerals are more resistant to the high-energy electron beam.

3) An exponential correlation between the ratio $I_{(i)}/I_{(Si)}$ and analytical measuring time was found to adequately describe the measurements: $I_{(i)}/I_{(Si)} = K_3 + K_1 e^{K_2 t}$.

4) Fractional element loss increases with decreasing specimen thickness.

https://doi.org/10.1346/CCMN.1998.0460309 Published online by Cambridge University Press

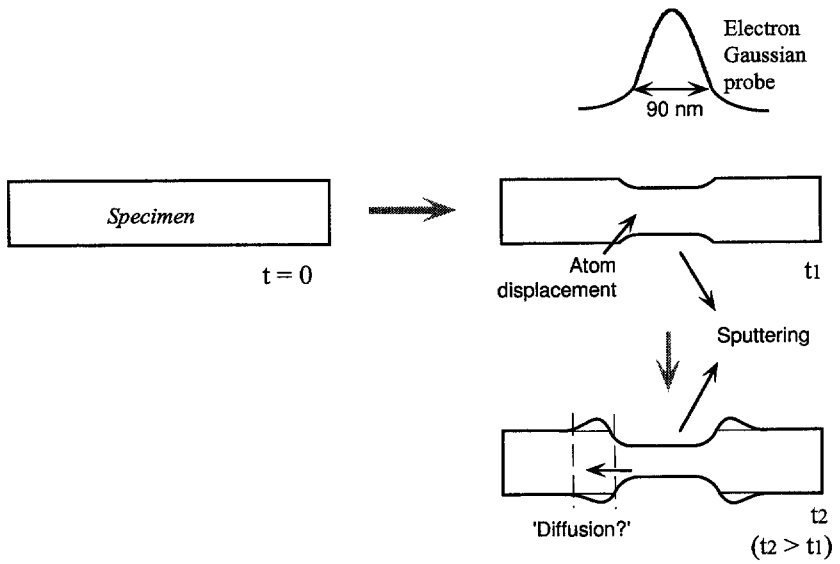

Figure 14. A diagram showing possible mechanisms for the loss of elements with time (t). The effect of electron distribution might contribute to the exponential relation between the $I_{(i)}/I_{(Si)}$ ratio and t. Sputtering and diffusion are likely to be the main causes for element losses.

5) A lower beam current and a larger analysis area reduce the loss of elements, which is particularly significant and important to clay minerals.
6) Most of the element loss takes place at the beginning of spectral collection, before statistically significant count totals can be obtained.
7) For phyllosilicates, including clay minerals, the loss of elements is also related to the specimen habit, loss of elements generally being more severe for thin crystals having a specimen plane perpendicular to (001).
8) The mechanism of "diffusion" used in some papers to explain the loss of elements in AEM analysis of phyllosilicates at 100 to 200 kV accelerating voltages is probably accompanied at 300 kV by sputtering and there may be other factors. Since the specific mechanism of "diffusion" is still to be established, we recommend using the more general term "element loss" instead.
9) At low temperature (around −130 °C), these analyses of phyllosilicates from electrons of 300-keV in-

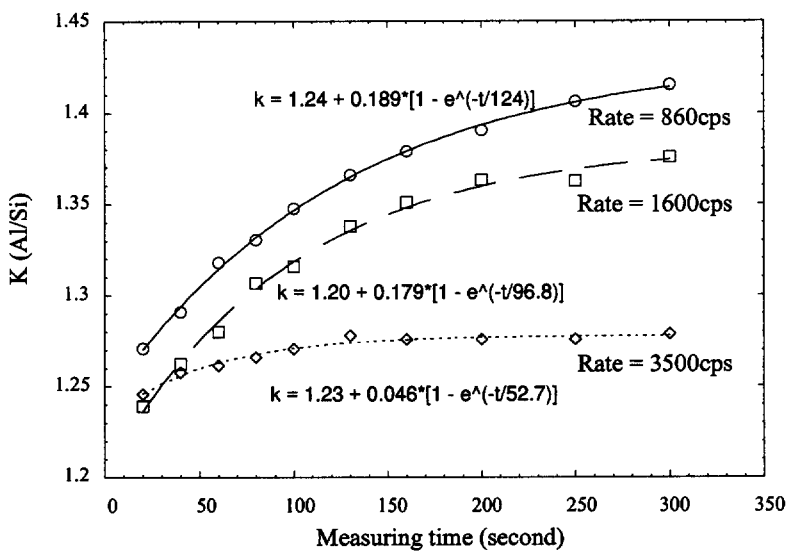

Figure 15. "Effective" k-factors from well-ordered kaolinite. Based on data from Figure 2.

https://doi.org/10.1346/CCMN.1998.0460309 Published online by Cambridge University Press

Table 2. The actual analysis of Pittong kaolinite (Kao I) and the AEM analysis using Methods 1 and 2.

Atomic ratio	Actual value†	Method 1	Method 1	Method 1	Method 2	Method 2	Method 2
Al/Si	1.025	1.021	1.035	1.024	0.936	0.945	0.965

† From Table 1.

cident energy showed that the loss of elements remained serious, in contrast to the results of Mackinnon and Kaser (1987) who also analyzed clays but used 200-keV electrons.

10) One should be aware that element loss during analysis is instrument-dependent. Before undertaking measurements of unknown clay crystals, one should use standard clay minerals (which have a similar structural ordering to unknown crystals) to calibrate an AEM instrument for "effective" *k*-factors of all elements for each mineral and to establish acceptable conditions for analysis (Method 1). Analysis of an unknown should be obtained under exactly the same conditions as were used for standards, including at least beam diameter, speciment thickness and total counting time for analysis. Although loss of elements occurs in both the standard and unknown, it should occur approximately equally in both and will be accounted for in the unknown's composition via the "effective" *k*-factor established from the standard.

ACKNOWLEDGMENTS

We wish to thank D. R. Peacor and I. D. R. Mackinnon for their thoughtful and constructive reviews on the manuscript. C. Ma also would like to thank G. R. Rossman for his helpful comments.

REFERENCES

Ahn JH, Peacor PR, Essene EJ. 1986. Cation-diffusion-induced characteristic beam damage in transmission electron microscope images of micas. Ultramicroscopy 19:375–382.

Cliff G, Lorimer GW. 1975. The quantitative analysis of thin specimens. J of Microscopy 103:203–207.

Knipe RJ. 1979. Chemical analysis during slaty cleavage development. Bull Mineral 102:206–210.

Lorimer GW, Cliff G. 1976. Analytical electron microscopy of minerals. In: Wenk HR, editor. Electron microscopy in mineralogy. Berlin: Springer. p 506–519.

Ma C. 1996. The ultra-structure of kaolin [Ph.D. thesis]. Canberra, Australia: Australian Nat Univ. 343 p.

Ma C, Eggleton RA. 1994. Structural characteristics of kaolin minerals from eastern Australian regolith. In: Pain CP, Craig MA, Campbell ID, editors. Abs Australian Regolith Conf; 1994; Broken Hill, Australia. p 40.

Mackinnon IDR. 1990. Low-temperature analyses in the analytical electron microscope. In: Mackinnon IDR, Mumpton FA, editors. Electron-optical methods in clay science. Boulder, CO: Clay Miner Soc. p 90–106.

Mackinnon IDR, Kaser SA. 1987. Microanalysis of clays at low temperature. In: Geiss RH, editor. Microbeam Analysis. San Francisco Press Inc. p 332–333.

Peacor DR. 1992. Analytical electron microscopy: X-ray analysis. In: Buseck PR, editor. Minerals and reactions at the atomic scale: Transmission electron microscopy. Washington, DC: Miner Soc Am. p 113–140.

Robertson IDM, Eggleton RA. 1991. Weathering of granitic muscovite to kaolinite and halloysite and of plagioclase-derived kaolinite to halloysite. Clays Clay Miner 39:113–126.

van der Pluijm BA, Lee JH, Peacor DR. 1988. Analytical electron microscopy and the problem of potassium diffusion. Clays Clay Miner 36:498–504.

Williams DB, Carter CB. 1996. Transmission electron microscopy: A textbook for materials science. New York: Plenum Pr. 729

(Received 4 August 1997; accepted 28 September 1997; Ms. 97-071).